HIGH ORDER MIXED FINITE ELEMENT DISCRETIZATION FOR THE VARIABLE EDDINGTON FACTOR EQUATIONS*

Samuel S. Olivier[1], Peter G. Maginot[2], and Terry S. Haut[3]

[1]Applied Science and Technology, University of California, Berkeley
Berkeley, CA 94708

[2] XCP-2 Eulerian Codes, Los Alamos National Lab
P.O. Box 1663, Los Alamos, NM 87545

[3]Center for Applied Scientific Computing, Lawrence Livermore National Lab
P.O. Box 7000, Livermore, CA 94551

solivier@berkeley.edu, pmaginot@lanl.gov, haut3@llnl.gov

ABSTRACT

This paper outlines a multi-dimensional, high-order, Mixed Finite Element discretization for the Variable Eddington Factor equations coupled to a high-order, upwind Discontinuous Galerkin S_N discretization. The resulting acceleration scheme is shown to maintain the order of accuracy of the S_N discretization in isolation, accelerate source iteration, and preserve the thick diffusion limit.

KEYWORDS: Variable Eddington Factor, Mixed Finite Element, Quasi Diffusion

1. INTRODUCTION

The Variable Eddington Factor (VEF) method, also known as Quasi-Diffusion (QD), was one of the first nonlinear methods for the acceleration of Discrete Ordinates (S_N) Source Iteration (SI) [1–3]. It is comparable in effectiveness to both linear and nonlinear forms of Diffusion Synthetic Acceleration (DSA) but offers much more flexibility. With DSA, stability can only be guaranteed when the diffusion equation is discretized in a "consistent" manner with the S_N discretization [4–7]. This can be problematic in the presence of advanced S_N discretizations, such as Discontinuous Galerkin (DG), where considerable effort has been placed into developing consistent DSA discretizations [8–11]. In addition, negative flux fixup schemes render any otherwise consistent, linear DSA scheme inconsistent which is likely to degrade convergence [4,12].

The primary advantage of the VEF method is that the VEF equations that accelerate source iteration do not need to be consistently discretized with respect to the S_N equations to remain effective.

*Reviewed for release as LLNL-CONF-773066

In fact, any valid discretization of the VEF equations will produce a conservative solution that inherently preserves the thick diffusion limit. In this "inconsistent" approach, the converged VEF and S_N scalar flux solutions differ by an amount proportional to the spatial truncation errors of the VEF and S_N discretizations. On a resolved mesh, this difference is on the order of the spatial truncation error and thus either solution is equally valid. Additionally, it is reasonable to expect that VEF's flexibility could extend to remaining effective even when negative flux fixup schemes are used making VEF an attractive multiphysics method.

This paper details a multi-dimensional, arbitrary order Mixed Finite Element Method (MFEM) discretization for the VEF equations coupled to an equally high order, upwind DG S_N discretization. This particular pairing is motivated by compatibility with the high order, mixed methods used for Arbitrary Lagrangian Eulerian (ALE) hydrodynamics as in [13]. Historically, it has been important to solve the hydrodynamics and radiation equations on the same mesh [14]. Furthermore, it is likely that using the same discretizations for radiation and hydrodynamics will lead to increased robustness, stability, and accuracy. A VEF method discretized in the same manner as the hydrodynamics equations is then clearly advantageous. Such a method would serve as an interface between the S_N and multiphysics discretizations and could potentially mitigate issues with solving the S_N equations on high-order (curved) meshes [11,15]. Mixed methods have been investigated for radiation diffusion in [16,17]. However, the presence of the VEF tensor places stricter continuity of current requirements at element interfaces leading to the discretization described here.

This combination was investigated in [18] in one-dimensional slab geometry using linear DG and lowest-order mixed finite elements. This work extends the method to both arbitrary order and 2/3 dimensions. The beneficial properties seen in one dimension namely preservation of the S_N order of accuracy, acceleration of SI, and preservation of the thick diffusion limit are verified in two dimensions.

2. VARIABLE EDDINGTON FACTOR ACCELERATION

Here, the VEF method will be described for a planar geometry, mono-energetic, fixed-source problem with isotropic scattering:

$$\hat{\Omega}\cdot\nabla\psi(\vec{x},\hat{\Omega})+\sigma_t\psi(\vec{x},\hat{\Omega})=\frac{\sigma_s}{4\pi}\int\psi(\vec{x},\hat{\Omega}')\,\mathrm{d}\Omega'+Q(\vec{x},\hat{\Omega})\,,\quad \vec{x}\in\mathcal{D}\,, \tag{1a}$$

$$\psi(\vec{x},\hat{\Omega})=\bar{\psi}(\vec{x},\hat{\Omega})\,,\quad \vec{x}\in\partial\mathcal{D}\ \text{ and }\ \hat{\Omega}\cdot\hat{n}<0\,, \tag{1b}$$

where the notation is standard. Applying the S_N angular discretization and lagging the scattering term:

$$\hat{\Omega}_d\cdot\nabla\psi_d^{\ell+1/2}(\vec{x})+\sigma_t\psi_d^{\ell+1/2}(\vec{x})=\frac{\sigma_s}{4\pi}\varphi^{\ell}+Q_d(\vec{x})\,,\quad d=1,\ldots,N_\Omega\,, \tag{2}$$

$$\psi_d(\vec{x})=\bar{\psi}(\vec{x},\hat{\Omega}_d)\,,\quad \vec{x}\in\partial\mathcal{D}\ \text{ and }\ \hat{\Omega}_d\cdot\hat{n}<0\,, \tag{3}$$

where $\{\hat{\Omega}_d,w_d\}_{d=1}^{N_\Omega}$ are stipulated by the S_N angular quadrature, $\psi_d(\vec{x})=\psi(\vec{x},\hat{\Omega}_d)$, $Q_d(\vec{x})=Q(\vec{x},\hat{\Omega}_d)$, and the superscripts indicate iteration index. The scalar flux is computed with:

$$\varphi^{\ell}(\vec{x})=\sum_{d=1}^{N_\Omega}w_d\psi_d^{\ell}(\vec{x}) \tag{4}$$

and is known either from the previous iteration or an initial guess when $\ell = 0$. Standard source iteration sets $\varphi^{\ell+1}(\vec{x}) = \varphi^{\ell+1/2}(\vec{x})$. However, this process exhibits arbitrarily slow convergence in optically thick, scattering dominated systems.

With VEF acceleration, transport information from iteration $\ell + 1/2$ is used to solve the VEF equations for an updated scalar flux:

$$\nabla \cdot \vec{J}(\vec{x}) + \sigma_a \phi^{\ell+1}(\vec{x}) = Q^{(0)}(\vec{x})\,, \tag{5a}$$

$$\nabla \cdot \left[\boldsymbol{E}\phi^{\ell+1}(\vec{x})\right] + \sigma_t \vec{J}(\vec{x}) = \vec{Q}^{(1)}(\vec{x})\,, \tag{5b}$$

$$\vec{J}(\vec{x}) \cdot \hat{n} = E_b \phi^{\ell+1}(\vec{x}) - 2J_{\text{in}}\,, \quad \vec{x} \in \partial\mathcal{D}\,, \tag{5c}$$

where $\vec{J}(\vec{x})$ is the current, $Q^{(0)}(\vec{x})$ the zeroth angular moment of the fixed-source, and $\vec{Q}^{(1)}(\vec{x})$ the first angular moment of the fixed-source. The VEF tensor, $\boldsymbol{E}$, and boundary factor, E_b, are computed using the angular flux from iteration $\ell + 1/2$ with:

$$\boldsymbol{E} = \frac{\sum_d \hat{\Omega}_d \otimes \hat{\Omega}_d \, \psi_d^{\ell+1/2}(\vec{x}) w_d}{\sum_d \psi_d^{\ell+1/2}(\vec{x}) w_d}\,, \tag{6}$$

$$E_b = \frac{\sum_d |\hat{\Omega}_d \cdot \hat{n}| \, \psi_d^{\ell+1/2}(\vec{x}) w_d}{\sum_d \psi_d^{\ell+1/2}(\vec{x}) w_d}\,, \tag{7}$$

and the incoming partial current on the boundaries is computed from the S_N boundary conditions as:

$$J_{\text{in}} = \sum_{\hat{\Omega}_d \cdot \hat{n} < 0} |\hat{\Omega}_d \cdot \hat{n}| \, \bar{\psi}(\vec{x}, \hat{\Omega}_d) w_d\,. \tag{8}$$

These equations and boundary conditions are the multi-dimensional analogs to those derived in detail in [18]. The VEF scalar flux is then used as the scattering source for the next iteration. This is repeated until successive iterates of the VEF scalar flux converge to within a specified tolerance.

3. DISCRETIZATIONS

This section describes the upwind DG S_N discretization, the MFEM VEF discretization, and the overlap between them occurring in the computation of the VEF tensor and construction of the S_N scattering source. It is assumed that S_N and VEF are solved on the same mesh such that an element e in the S_N discretization occupies the same space as the element e in the VEF discretization.

3.1. Discontinuous Galerkin S_N

The S_N equations are spatially discretized using an arbitrary order, upwind DG discretization as in [11,15,19]. In DG, the angular flux is approximated *locally* on each element with

$$\psi_d^e(\vec{x}) \approx \sum_{j=1}^{N_\psi} b_j^e(\vec{x}) \psi_{d,j}^e\,, \tag{9}$$

where $\{b_j^e\}_{j=1}^{N_\psi}$ is a set of Lagrange finite element basis functions defined on the element e. For tensor product elements (quadrilaterals and hexahedrals), these basis functions span Q_p, the space

of all polynomials of degree at most p in each variable. On a face $\Gamma_{e,e'}$ between neighboring elements e and e', upwinding is used to uniquely define the angular flux:

$$\psi_d(\vec{x}) = \begin{cases} \psi_d^e(\vec{x}), & \hat{\Omega}_d \cdot \hat{n}_e \geq 0 \\ \psi_d^{e'}(\vec{x}), & \hat{\Omega}_d \cdot \hat{n}_e < 0 \end{cases}, \quad \vec{x} \in \Gamma_{e,e'}. \tag{10}$$

The standard Galerkin procedure produces the following discretization:

$$[\mathbf{G}_d + \mathbf{F}_d + \mathbf{M}_t]\,\underline{\psi_d} = \mathbf{M}_s \underline{\varphi} + \boldsymbol{q}_d, \tag{11}$$

where we have assumed the notation and definitions of [11]. The angular flux solution is then used to compute the VEF tensor in each element as

$$\boldsymbol{E}^e = \frac{\sum_j^{N_\psi} b_j^e(\vec{x}) \sum_d^{N_\Omega} \hat{\Omega}_d \otimes \hat{\Omega}_d \, \psi_{d,j}^e w_d}{\sum_j^{N_\psi} b_j^e(\vec{x}) \sum_d^{N_\Omega} \psi_{d,j}^e w_d}, \tag{12}$$

where the spatial variance of the VEF tensor is inherited from the interpolation of the angular flux. Note that the numerator and denominator are interpolated independently and thus the VEF tensor is a rational polynomial in space.

3.2. Mixed Finite Element VEF Discretization

Testing the VEF equations with $(u, \vec{v}) \in L^2(\mathcal{D}) \times \vec{H}^1(\mathcal{D})$, the weak form is: find $(\phi, \vec{J}) \in L^2(\mathcal{D}) \times \vec{H}^1(\mathcal{D})$ such that

$$\int_{\mathcal{D}} u \nabla \cdot \vec{J} \,\mathrm{d}V + \int_{\mathcal{D}} u \sigma_a \phi \,\mathrm{d}V = \int_{\mathcal{D}} u Q^{(0)} \,\mathrm{d}V, \tag{13a}$$

$$-\int_{\mathcal{D}} \nabla \vec{v} : \boldsymbol{E}\, \phi \,\mathrm{d}V + \int_{\mathcal{D}} \sigma_t \vec{v} \cdot \vec{J} \,\mathrm{d}V = \int_{\mathcal{D}} \vec{v} \cdot \vec{Q}^{(1)} \,\mathrm{d}V - \int_{\partial\mathcal{D}} \vec{v} \cdot \boldsymbol{E} \cdot \hat{n}\, \bar{\phi} \,\mathrm{d}A, \tag{13b}$$

holds for all $(u, \vec{v})$ where $\phi = \bar{\phi}$ on $\partial\mathcal{D}$. In the above, Green's Identity:

$$\int_{\mathcal{D}} \vec{v} \cdot \nabla \cdot (\boldsymbol{E}\phi) \,\mathrm{d}V = \int_{\partial\mathcal{D}} \vec{v} \cdot \boldsymbol{E} \cdot \hat{n}\, \phi \,\mathrm{d}A - \int_{\mathcal{D}} \nabla \vec{v} : \boldsymbol{E}\, \phi \,\mathrm{d}V, \tag{14}$$

was used since $\nabla \cdot (\boldsymbol{E}\phi)$ is not square integrable. The presence of the gradient of $\vec{v}$ in the first moment equation precludes the use of $H(\mathrm{div})$ finite elements as the gradient of an $H(\mathrm{div})$ function violates the De Rham complex. This is the motivation for approximating the current with $\vec{H}^1(\mathcal{D})$ instead of $H(\mathrm{div})$ which has been shown to be effective for radiation diffusion in mixed form [16].

The finite element procedure is then to approximate ϕ and $\vec{J}$ in finite-dimensional subspaces of $L^2(\mathcal{D})$ and $\vec{H}^1(\mathcal{D})$, respectively:

$$\phi(\vec{x}) \approx \sum_j^{N_\phi} B_j(\vec{x}) \phi_j, \quad B_j(\vec{x}) \subset L^2(\mathcal{D}), \tag{15}$$

$$J_i(\vec{x}) \approx \sum_j^{N_J} N_j(\vec{x}) J_{i,j}, \quad N_j(\vec{x}) \subset H^1(\mathcal{D}). \tag{16}$$

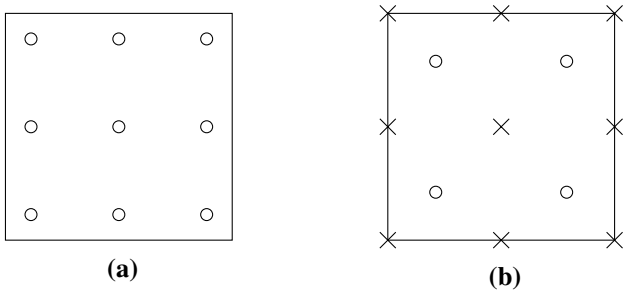

Figure 1: The distribution of nodes in a (a) quadratic DG element and (b) the corresponding Q_2Q_1 mixed element. The exes denote current nodes and the circles scalar flux nodes.

In other words, each component of the current is interpolated independently with $H^1(\mathcal{D})$ basis functions. This can be written as:

$$\vec{J}(\vec{x}) \approx \sum_{j}^{dim \times N_J} \vec{N}_j(\vec{x}) J_j \,, \quad \vec{N}_j(\vec{x}) \subset \vec{H}^1(\mathcal{D}) \,, \tag{17}$$

where each $\vec{N}_j(\vec{x})$ has one component equal to an $H^1(\mathcal{D})$ basis function and the rest zero.

For tensor product elements, $\{B_j\}$ spans Q_k. Stability mandates that the current basis functions span Q_{k+1} and are thus one polynomial order higher than the scalar flux polynomial order. This $Q_{k+1}Q_k$ discretization converges as h^{k+2}. Thus, to match DG's h^{p+1} convergence, k is chosen to be $p-1$. For example, Fig. 1 shows the distribution of nodes for a quadratic DG element and the corresponding Q_2Q_1 element. Interpolation between the Q_p and Q_{p-1} spaces is handled natively by the finite element procedure. Since the S_N and VEF meshes are identical, Eq. 12 can be used directly to evaluate the VEF tensor throughout the domain.

Applying Galerkin's method where $(u, \vec{v})$ are approximated with the same interpolations as $(\phi, \vec{J})$ yields the following block system:

$$\begin{bmatrix} \mathbf{M}_t & \mathbf{G}_E \\ \mathbf{D} & \mathbf{M}_a \end{bmatrix} \begin{bmatrix} \underline{J} \\ \underline{\phi} \end{bmatrix} = \begin{bmatrix} \boldsymbol{g} \\ \boldsymbol{f} \end{bmatrix} \,, \tag{18}$$

where the global matrices and vectors above are defined as:

$$\begin{aligned} &[\mathbf{M}_t]_{ij} = \int \sigma_t \vec{N}_i \cdot \vec{N}_j \,\mathrm{d}V \,, && [\mathbf{G}_E]_{ij} = -\int \nabla \vec{N}_i : \boldsymbol{E} B_j \,\mathrm{d}V \,, \\ &[\mathbf{D}]_{ij} = \int B_i \nabla \cdot \vec{N}_j \,\mathrm{d}V \,, && [\mathbf{M}_a]_{ij} = \int \sigma_a B_i B_j \,\mathrm{d}V \,, \\ &[\boldsymbol{g}]_i = \int \vec{N}_i \cdot \vec{Q}^{(1)} \,\mathrm{d}V - \textstyle\int_{\partial\mathcal{D}} \vec{N}_i \cdot \boldsymbol{E} \cdot \hat{n}\, \bar{\phi} \,\mathrm{d}A \,, && [\boldsymbol{f}]_i = \int B_i Q^{(0)} \,\mathrm{d}V \,. \end{aligned} \tag{19}$$

In practice, the current basis functions are used as an isoparametric map to a reference element where Gaussian Quadrature can be easily applied. Boundary conditions are applied by solving Eq. 5c for the scalar flux and substituting the result for $\bar{\phi}$ in the boundary term of the $\boldsymbol{g}$ vector. This introduces an additional bilinear form and modified linear form (included as additions to $\mathbf{M}_t$ and

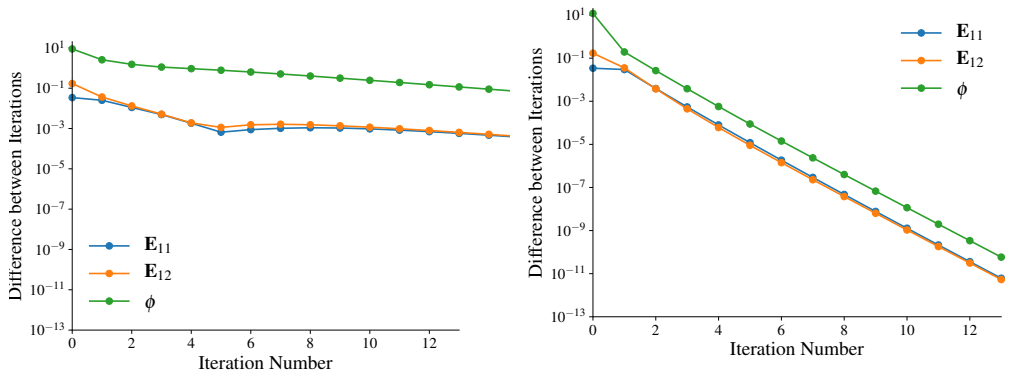

Figure 2: The L^∞ difference between successive iterates of two components of the VEF tensor and the scalar flux for (a) unaccelerated SI and (b) the VEF method.

$\boldsymbol{g}$ for brevity):

$$[\mathbf{M}_t]_{ij} = \int \sigma_t \vec{N}_i \cdot \vec{N}_j \, \mathrm{d}V + \int_{\partial\mathcal{D}} \frac{1}{E_b} \left(\vec{N}_i \cdot \boldsymbol{E} \cdot \hat{n}\right) \left(\vec{N}_j \cdot \hat{n}\right) \mathrm{d}A \,, \tag{20}$$

$$[\boldsymbol{g}]_i = \int \vec{N}_i \vec{Q}^{(1)} \, \mathrm{d}V - \int_{\partial\mathcal{D}} \frac{2}{E_b} \vec{N}_i \cdot \boldsymbol{E} \cdot \hat{n} \, J_{\text{in}} \, \mathrm{d}A \,. \tag{21}$$

Note that due to the discontinuous nature of the scalar flux approximation, the absorption mass matrix is block-diagonal. Thus, its inverse can be computed and stored efficiently without fill-in. The Schur complement can then be formed to solve a smaller system of the current unknowns only:

$$\left[\mathbf{M}_t - \mathbf{G}_E \mathbf{M}_a^{-1} \mathbf{D}\right] \underline{J} = \boldsymbol{g} - \mathbf{G}_E \mathbf{M}_a^{-1} \mathbf{D} \boldsymbol{f} \,, \tag{22}$$

$$\underline{\phi} = \mathbf{M}_a^{-1} [\boldsymbol{f} - \mathbf{D} \underline{J}] \,, \tag{23}$$

where the Schur Complement $\mathbf{S} = \mathbf{M}_t - \mathbf{G}_E \mathbf{M}_a^{-1} \mathbf{D}$ is not symmetric since $\mathbf{G}_E \neq \mathbf{D}^T$ due to the presence of the VEF tensor. Unfortunately, the Schur complement system has been difficult to solve iteratively necessitating the use of sparse direct methods.

Once the VEF system is solved, the S_N elemental scattering mass matrix is computed with:

$$[\mathbf{M}_s^e]_{ij} = \int_{\kappa_e} \frac{\sigma_s}{4\pi} b_i^e B_j^e \, \mathrm{d}V \,. \tag{24}$$

Multiplying this mass matrix by the VEF scalar flux nodal values produces the scattering source for the next S_N solve, completing the iteration.

4. RESULTS

This section applies the VEF method described above to several fixed-source problems to demonstrate the effectiveness of the method. Our implementation of the VEF algorithm utilizes the

Table 1: The number of iterations required for convergence over a range of ϵ.

ϵ	1×10^{-1}	1×10^{-2}	1×10^{-3}	1×10^{-4}	1×10^{-5}
N_{iter}	10	6	4	3	3

MFEM finite element library [20]. All problems were solved on a $1\,\text{cm} \times 1\,\text{cm}$ orthogonal, uniformly spaced mesh of quadrilaterals using S_8 angular quadrature. The scalar fluxes were converged in the L^∞ norm to a tolerance of 1×10^{-10}. Unless otherwise noted, the domain was 10 mfp thick and quadratic DG with Q_2Q_1 VEF was used.

Figure 2 shows the difference between successive iterates (measured in the L^∞ norm) of two components of the VEF tensor and the scalar flux for unaccelerated SI and the VEF method. The scattering ratio was $c = 0.99$ and vacuum boundary conditions were applied on all faces. In the unaccelerated case, the VEF tensor is approximately two orders of magnitude more converged than the scalar flux at every iteration. When VEF acceleration is used, the fast convergence of the VEF tensor is transferred to the scalar flux resulting in a rapidly convergent algorithm.

The Method of Manufactured Solutions (MMS) was applied to verify that our VEF method maintains the order of accuracy of the DG S_N discretization in isolation. Let,

$$\psi_d(\vec{x}) = \left(1 + \mu_d^2\right) \sin\left(\pi \frac{x+\alpha}{L+2\alpha}\right) \sin\left(\pi \frac{y+\alpha}{L+2\alpha}\right) \tag{25}$$

where $L = 1\,\text{cm}$ is the length of the domain and $\alpha = 0.1$ allows the inflow boundary conditions to be tested. The MMS source is then:

$$Q_d = \left(1 + \mu_d^2\right) \frac{\pi}{L+2\alpha} \left[\mu \cos\left(\pi \frac{x+\alpha}{L+2\alpha}\right) \sin\left(\pi \frac{y+\alpha}{L+2\alpha}\right) + \eta \sin\left(\pi \frac{x+\alpha}{L+2\alpha}\right) \cos\left(\pi \frac{y+\alpha}{L+2\alpha}\right)\right] + \sigma_t \psi_d(\vec{x}) - \frac{\sigma_s}{4\pi} \sum_{d'=1}^{N_\Omega} \psi_{d'}(\vec{x}) w_{d'} \,. \tag{26}$$

This process produces an exact angular and scalar flux that can be compared as the mesh is refined. Figure 3 shows the L^2 error between the VEF scalar flux and the exact MMS scalar flux as the mesh is refined. Three finite element orders were tested: linear DG with Q_1Q_0 VEF, quadratic DG with Q_2Q_1 VEF, and cubic DG with Q_3Q_2 VEF. The error converges as h^{p+1} as expected from the DG discretization.

Next, the acceleration effectiveness was evaluated by varying the scattering ratio in the 10 mfp square domain. Figure 4 shows the number of iterations required for convergence for unaccelerated SI and VEF as the scattering ratio is varied between $c \in [1 \times 10^{-6}, 0.9999]$. VEF was effective for all values of c and led to a $100\times$ reduction in iterations for $c = 0.9999$.

Finally, the method was tested in the thick diffusion limit by scaling the cross sections and source according to:

$$\sigma_t = \frac{10\,\text{cm}^{-1}}{\epsilon}\,, \quad \sigma_a = \epsilon\left(5\,\text{cm}^{-1}\right)\,, \quad Q = \epsilon\left(1\,\text{cm}^{-2}\,\text{sr}^{-1}\right) \tag{27}$$

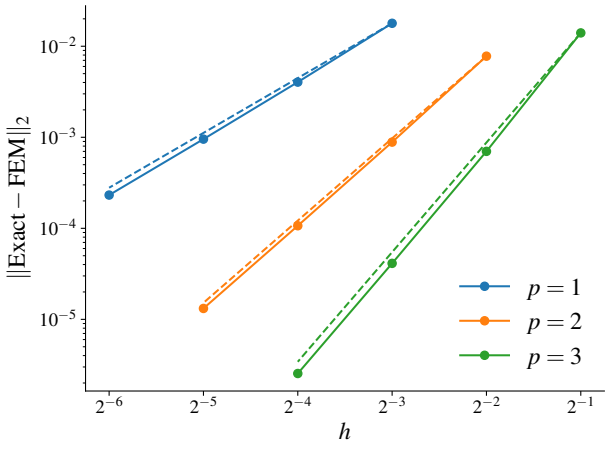

Figure 3: The numerical error for a range of mesh sizes for linear, quadratic, and cubic VEF with corresponding reference lines of slope $p + 1$.

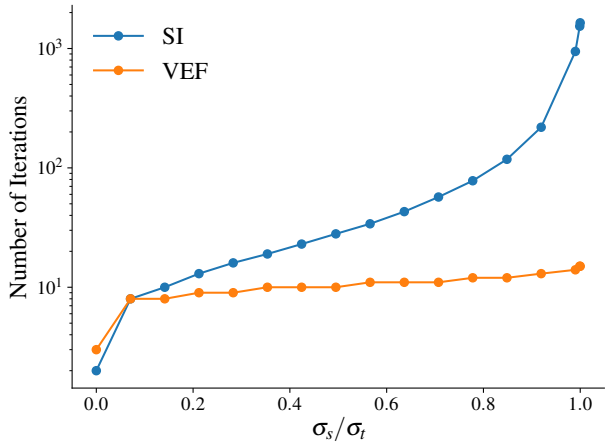

Figure 4: The number of iterations until convergence for SI and VEF as the scattering ratio is varied.

in the limit as $\epsilon \to 0$. The number of iterations until convergence is shown in Table 1 for a range of ϵ. This shows that the VEF method preserves the thick diffusion limit.

5. CONCLUSIONS

This paper outlines a multi-dimensional, high-order, Mixed Finite Element discretization for the Variable Eddington Factor equations coupled to a high-order Discontinuous Galerkin S_N discretization. It was shown that this coupling preserves the order of accuracy of the S_N discretization in isolation, greatly reduces the number of iterations required for convergence in optically thick systems, and preserves the thick diffusion limit.

In the future, hybridization of the discretized VEF linear system will be pursued as it is likely to produce a system more amenable to iterative solvers. The method is also showing promising results in accelerating SI when negative flux fixups are applied to the angular flux. Ultimately, this work will be extended to the Thermal Radiative Transfer equations where the discretization flexibility demonstrated here will be useful when solving on high-order, curvilinear meshes.

ACKNOWLEDGEMENTS

This research is supported by the Department of Energy Computational Science Graduate Fellowship, provided under grant number DE- SC0019323 and was performed under the auspices of the U.S. Department of Energy by Lawrence Livermore National Laboratory under Contract DE-AC52-07NA27344.

REFERENCES

[1] M. Adams and E. Larsen. "Fast Iterative Methods for Discrete-Ordinates Particle Transport Calculations." *Progress in Nuclear Energy*, **volume 40**(1), pp. 3–159 (2002).

[2] D. Mihalas. *Stellar Atmospheres*. W. H. Freeman and Co (1978).

[3] V. Ya. Gol'din. "A Quasi-Diffusion Method of Solving the Kinetic Equation." *USSR Comp Math and Math Physics*, **volume 4**, pp. 136–149 (1964).

[4] R. Alcouffe. "Diffusion Synthetic Acceleration Methods for the Diamond-Differenced Discrete-Ordinates Equations." *Nuclear Science and Engineering*, **volume 64**, pp. 344–355 (1977).

[5] W. H. Reed. "The effectiveness of acceleration techniques for iterative methods in transport theory." *Nuclear Science and Engineering*, **volume 45**(3), pp. 245–254 (1971).

[6] E. M. Gelbard and L. A. Hageman. "The synthetic method as applied to the S_N equations." *Nuclear Science and Engineering*, **volume 37**(2), pp. 288–298 (1969).

[7] E. W. Larsen. "The asymptotic diffusion limit of discretized transport problems." *Nuclear Science and Engineering*, **volume 112**, pp. 336–346 (1992).

[8] J. Warsa, T. Wareing, and J. Morel. "Fully-Consistent Diffusion-Synthetic Acceleration of Linear Discontinuous S_N Transport Discretizations on Unstructured Tetrahedral Meshes." *Nuclear Science and Engineering*, **volume 141**, pp. 235–251 (2002).

[9] M. L. Adams and W. R. Martin. "Diffusion Synthetic Acceleration of Discontinuous Finite Element Transport Iterations." *Nuclear Science and Engineering*, **volume 111**, pp. 145–167 (1992).

[10] Y. Wang and J. C. Ragusa. "Diffusion Synthetic Acceleration for High-Order Discontinuous Finite Element S_N Transport Schemes and Application to Locally Refined Unstructured Meshes." *Nuclear Science and Engineering*, **volume 166**(2), pp. 145–166 (2010).

[11] T. S. Haut, B. S. Haut, P. G. Maginot, and V. Z. Tomov. "DSA Preconditioning for DG Discretizations of S_N Transport and High-Order Curved Meshes." *submitted* (2019).

[12] E. D. Fichtl, J. S. Warsa, and J. D. Densmore. "The Newton-Krylov Method Applied to Negative-Flux Fixup in SN Transport Calculations." *Nuclear Science and Engineering*, **volume 165**(3), pp. 331–341 (2010).

[13] V. Dobrev, T. Kolev, and R. Rieben. "High-Order Curvilinear Finite Element Methods for Lagrangian Hydrodynamics." *SIAM Journal on Scientific Computing*, **volume 34**, pp. B606–B641 (2012).

[14] J. A. Rathkopf et al. "KULL: LLNL's ASCI inertial confinement fusion simulation code." *PHYSOR 2000 American Nuclear Society Topical Meeting on Advances in Reactor Physics and Mathematics and Computation in the Next Millenium* (May 7-11 2000).

[15] T. S. Haut, P. G. Maginot, V. Z. Tomov, B. S. Southworth, T. A. Brunner, and T. S. Bailey. "An Efficient Sweep-Based Solver for the SN Equations on High-Order Meshes." *Nuclear Science and Engineering* (2019).

[16] P. G. Maginot and T. A. Brunner. "Lumping Techniques for Mixed Finite Element Diffusion Discretizations." *Journal of Computational and Theoretical Transport*, **volume 47**(4-6), pp. 301–325 (2018).

[17] J. S. Warsa, M. Benzi, T. A. Wareing, and J. E. Morel. "Preconditioning a mixed discontinuous finite element method for radiation diffusion." *Numerical Linear Algebra with Applications*, **volume 11**, pp. 795–811 (2004).

[18] S. S. Olivier and J. E. Morel. "Variable Eddington Factor Method for the SN Equations with Lumped Discontinuous Galerkin Spatial Discretization Coupled to a Drift-Diffusion Acceleration Equation with Mixed Finite-Element Discretization." *Journal of Computational and Theoretical Transport*, **volume 46**(6-7), pp. 480–496 (2017). URL https://doi.org/10.1080/23324309.2017.1418378.

[19] J. L. Guermond, G. Kanshat, and J. C. Ragusa. "Discontinuous Galerkin methods for the radiative transport equation." *The IMA Volumes in Mathematics and its Applications*, **volume 157**, pp. 181–193 (2014).

[20] "MFEM: Modular Finite Element Methods Library." mfem.org.